In situ X-ray reflectivity and GISAXS study of mesoporous silica films grown from sodium silicate solution precursors

Andi Di, Julien Schmitt, Naomi Elstone, Thomas Arnold, Karen J Edler

Microporous and Mesoporous Materials 341 (2022) 112018

Contents lists available at ScienceDirect

Microporous and Mesoporous Materials

journal homepage: www.elsevier.com/locate/micromeso

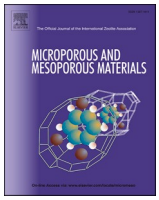

In situ X-ray reflectivity and GISAXS study of mesoporous silica films grown from sodium silicate solution precursors

Andi Di [a], Julien Schmitt [a,b], Naomi Elstone [a], Thomas Arnold [a,c,d], Karen J. Edler [a,*]

[a] *Department of Chemistry, University of Bath, Claverton Down, Bath, Avon, BA2 7AY, UK*
[b] *LSFC- Laboratoire de Synthèse et Fonctionnalisation des Céramiques, UMR 3080 CNRS / Saint-Gobain CREE, Saint-Gobain Research Provence, 550 avenue Alphonse Jauffret, Cavaillon, France*
[c] *Diamond Light Source, Harwell Campus, Didcot, OX11 0DE, UK*
[d] *European Spallation Source ERIC, P.O Box 176, SE-221 00, Lund, Sweden*

A B S T R A C T

An environmentally friendly and inexpensive silica source, sodium silicate solution, was applied to synthesize a free-standing mesoporous silica film at the air/liquid interface, exploiting the co-assembly of cetyltrimethylammonium bromide and polyethylenimine. The effect of the composition of the solution used for the film formation on the mesostructure of the as-synthesized silica films, characterized by small angle X-ray scattering (SAXS), was investigated. The initial film formation time is estimated by the change in surface pressure with time. Additionally, a possible formation process of the mesostructured silica film is proposed using data from *in situ* grazing incidence small angle X-ray scattering (GISAXS) and X-ray reflectivity (XRR) measurements. A free-standing film with a wormlike structure was formed at the interface and reorganized into a 2D hexagonal ordered structure while drying at room temperature, after removal from the air/solution interface. The ordered 2D hexagonal structure, however, could only be retained to some extent during calcination, in samples where nitrate ions are present in the film formation solution.

1. Introduction

Ordered mesostructured silica materials have been extensively studied due to their applications in separation, and catalysis [1–6]. The synthesis [7,8], formation mechanism [9,10], and characterization [11] of ordered silica materials with various morphologies (powders, monoliths, fibres *etc.*) [12–14] have been well established. However, demand for chemical sensors and separation have stimulated the exploration of ordered mesoporous silica materials in thin-film geometry [15–18].

Soft templating methods, using organic species as the structure-directing agents, are widely used to prepare mesoporous silica films. The open framework, tunable porosities and surface areas [19–22] endow the prepared silica film with accessibility to reagents and metal ions, which is of vital importance in the fields of chemical sensors and separation. Electrochemically assisted self-assembly (EASA) [23,24] and evaporation-induced self-assembly (EISA) [25,26], are the most widely used methods to synthesize mesoporous silica films. The EASA methods require conducting supports to guarantee a cathodic potential [23]. The EISA methods, e.g. spin coating and dip coating, also need substrates for coating and are highly humidity-dependent [26–28]. Alternatively, the free-standing film formation method produces thin films at the air/-solution interface. The film formation process can be probed *in situ* by several techniques, e.g. surface pressure, grazing incidence small angle scattering, and X-ray/neutron reflectivity. These techniques give valuable insight into the structural evaluation of the film at the interface but are not applicable to bulk materials. Tremendous research effort has been put into the synthesis and application of continuous free-standing mesostructured silica films grown at the air/solution interface since Yang et al. first reported the synthesis of mesoporous silica films using cetyltrimethylammonium chloride as the structure-directing agent under acidic conditions [29,30].

Films templated by surfactant-polyelectrolyte complexes are much more flexible and resistant to cracking than those containing only surfactants and silica, allowing easier subsequent manipulation and calcination. This method also allows tuning the pore size of the silica films [31]. Polyethylenimine (PEI), a positively charged polyelectrolyte, was reported to form free-standing films when mixed with cetyltrimethylammonium bromide (CTAB) in water [32]. The aggregation of the CTAB-PEI complexes was reported to be favoured by electrostatic interactions, hydrophobic interactions, and charge-dipole interactions [33–35]. The formation of CTAB-PEI films is based on the aggregation of the CTAB-PEI complex at the air-solution interface driven by the evaporation of solvent [36], and it can be used to synthesize free-standing silica films in presence of tetramethoxysilane (TMOS) [37]. A modified method, involving anionic sodium dodecyl sulfate (SDS) in the

* Corresponding author.
E-mail address: k.edler@bath.ac.uk (K.J. Edler).

https://doi.org/10.1016/j.micromeso.2022.112018
Received 26 January 2022; Received in revised form 16 May 2022; Accepted 23 May 2022
Available online 25 May 2022

CTAB-PEI system to prepare CTAB-SDS-PEI templated free-standing mesoporous silica film under alkaline conditions, was also investigated [31,38]. TMOS, an alkoxysilane precursor, used in this earlier work, although convenient as a model system, is not suitable for scale-up due to its toxicity and expense [39]. Besides, methanol generated during the hydrolysis process disrupts the micelle organization, affecting the control of the mesostructure, the thickness and the strength of the prepared films. Using more TMOS to provide further silica to strengthen the network could not solve this problem since the amount of methanol generated dissolved the micelles. Sodium silicate solution (Na-silicate), which produces no organic species during polymerization, is a potential candidate to avoid these drawbacks. However, for acidic systems [40,41], where Na-silicate precipitates, only alkoxysilane precursors could be used. This CTAB-PEI templating approach is unique in allowing the silica film to grow from alkaline solutions, permitting the use of Na-silicate. The use of Na-silicate also has the potential to achieve thicker films and overall stronger membranes. Therefore, we have investigated the synthesis of films using an aqueous Na-silicate as the silica source. The effect of the composition of the film formation solution on the mesostructure of the silica films was investigated to determine the important factors responsible for production of ordered mesostructures and robust films. Moreover, a possible mesostructure formation route is drawn according to the *in situ* X-ray reflectivity and GISAXS data.

2. Experimental section

2.1. Materials and methods

Branched polyethylenimine (Mw = 750 000, denoted as LPEI, 50 w/v% in H_2O, analytical grade), sodium silicate solution (Na-silicate, $(NaOH)_x(Na_2SiO_3)_y{\cdot}zH_2O$; 13.4–14.4 wt % NaOH; 12.0–13.0 wt % Si; density = 1.39 g/mL at 25 °C), sodium hydroxide (NaOH, purity >98%) sodium nitrate (ACS reagent, purity >99.0%), and sodium dodecyl sulfate (SDS, purity >98.5%) were purchased from Sigma-Aldrich. Cetyltrimethylammonium bromide (CTAB, purity >99.0%) was purchased from ACROS Organic. All the chemicals were used as received without further purification. Milli-Q water (18.2 MΩ cm^{-1} resistance, from an ELGA PURELAB flex water purification system) was used as the solvent.

2.2. Synthesis

The film synthesis procedure is a modified version of that reported earlier [31,37]. In a standard preparation, solutions of surfactants (a singular surfactant system CTAB or a binary surfactant system CTAB-SDS), LPEI and NaOH were mixed using a magnetic stirrer to obtain a 30 ml solution (pH ~ 12.8). The molar concentrations in the solution were [CTAB] = 37.0 mM, [LPEI] = 0.3 mM and [NaOH] = 100.0 mM, respectively. In the case of the binary surfactant system, the concentration of CTAB remained at 37.0 mM, while [SDS] = 3.0 mM. Subsequently, Na-silicate solution, with a final Na-silicate concentration varying from 10.7 to 86.3 mM, was added dropwise and the mixture was stirred until homogeneous.

The mixture was transferred into a petri dish with a piece of plastic mesh floating on the solution surface (Fig. S1) and was left to reach a quiescent state. The growth of the mesostructured silica film was typically allowed to proceed for 24 h at room temperature (*ca.* 21 °C). The film was captured by drawing the mesh out from the interface and the mesh was then hung on a hook to dry at room temperature. Small pieces of film were obtained after calcination at 600 °C for 6 h with and without a pretreatment strategy before calcination. The pretreatment involves the removal of NaOH and excess structure-directing agents through washing with 10 mL Milli-Q water, drying for 6 h at 45 °C and a pre-calcination step at 100 °C for 12 h.

2.3. Characterization

The mesostructure of the as-prepared and calcined silica films was characterized by small angle X-ray scattering (SAXS), using an Anton Paar SAXSess instrument with a Panalytical PW3830 X-ray generator at 40 kV and 50 mA, which gives a Q range between 0.08 $Å^{-1}$ and 2.7 $Å^{-1}$. Scattered X-rays (Cu K_α) were detected by a reusable Europium excitation based image plate (size: 66 × 200 mm) with a 42.3 μm^2 pixel size. The image plate was subsequently read by a Perkin Elmer Cyclone reader using OptiQuant software. SAXS profiles were generated from the 2D image using the Anton Paar SAXSquant program.

The changes of surface pressure with time were recorded by using a glass fibre (diameter: 0.777 mm) hung from a microbalance sensor (type PS4, Nima Technology), connected to the Nima software. Measurement of the fibre in air was used to zero the sensor. The measurement started at the point when the film formation solution was poured into the Langmuir trough with sufficient height to touch the fibre.

X-ray reflectivity (XRR) and grazing incident small angle X-ray scattering (GISAXS) measurements were made using the DCD system [42] at the I07 beamline [43] at the Diamond Light Source (Didcot, Oxfordshire, UK). The X-ray energy was 12.5 keV. Teflon troughs containing film formation solutions were placed on a sample holder and sealed using a plastic box with a Kapton window to allow the beam to go through. Helium gas flowed through the box to reduce the scattering from air. The measurements were conducted at room temperature (*ca.* 21 °C). Data were collected using a Pilatus 100 K detector using regions of interest for reflected intensity and background. Data were reduced using the DAWN software package [44], including a geometric footprint correction for over-illumination. The data are displayed as scattering intensity against the momentum transfer, Q. The XRR measurements are sensitive to the differences in electron density normal to the surface of the growing film, while GISAXS provides structural information about the lateral surfaces [45].

Thermogravimetric analysis (TGA) of the prepared silica films was performed on a SETSYS Evolution TGA 16/18 thermogravimetric analyser (Setaram) from room temperature up to 650 °C, at a heating rate of 1 °C/min with airflow. The TGA data are displayed as the loss of weight as a percentage against temperature in °C.

Nitrogen sorption was measured at 77 K using a BELSORP instrument (BELSORP-mini Inc. Japan). The samples were degassed under vacuum at 523 K for 1000 min before measurements. The surface areas of the materials were calculated using the Brunauer-Emmett-Teller (BET) method.

Solutions of 37.0 mM CTAB aqueous solution in the presence of different $NaNO_3$ concentrations were measured at room temperature using dynamic light scattering (DLS) in a Malvern Zetasizer Nano ZSP instrument (Malvern, UK). All samples were filtered through a 0.45 μm filter (Millex-HA) to remove any dust before the measurements. Samples were measured at a scattering angle of 173° and a wavelength of 632.8 nm for 120 s, repeated 5 times. The size distribution, weighted in volume, was extracted using the CONTIN method.

3. Results and discussion

CTAB-LPEI-Silica films were successfully synthesized at the interface and could be removed intact on an open mesh. However, mixed surfactant CTAB/SDS-LPEI mixtures [31,37] were not effective to produce structured films in this case, since the produced film has a poorly ordered structure, indicated by the SAXS pattern in Fig. S2. This can be understood by considering the polymerization and condensation processes of the sodium silicate solution (Na-silicate). Na-silicates have been reported to polymerize via anionic oligomers under alkaline conditions [46,47], which will be electrostatically repelled by the anionic SDS molecules in the binary SDS-CTAB system. Additionally, SDS molecules in the system also reduce the charge on the cationic micelles formed by CTAB, consequently weaken the dipole-cationic interactions

between LPEI and surfactants [37], and compete with the anionic silica species to interact directly with the nitrogen groups in the LPEI. Thus, we focus only on the CTAB-LPEI-silica system in this work. The concentrations of the different film components were varied in turn to ascertain the most important factors to achieve thick mesostructured films which could be removed from the solution interface intact for further processing.

3.1. Effect of the concentration of silica source on CTAB-LPEI-silica films

The effect of the concentration of Na-silicate, expressed as molar concentration of SiO_2 in the film growth solution, on the structures formed at the solution interface with CTAB-PEI was studied at a constant CTAB-PEI concentration of 37.0 mM and 0.3 mM, respectively. As illustrated in Fig. 1, SAXS patterns of the ambient dried CTAB-PEI-silica films present four diffraction peaks when the SiO_2 concentration in the film growth solutions was 43.0, 65.0 and 86.3 mM. A sharp peak appears at around 0.16 $Å^{-1}$ along with a broad peak with low intensity at around 0.28 $Å^{-1}$. These positions are in the ratio of 1:1.73, correlated to the (100) and (110) diffraction peaks of the 2D hexagonal structure of close packed cylindrical micelles. The peaks located at around 0.24 and 0.48 $Å^{-1}$ are indexed to crystalline CTAB in the dry films [37]. At the lowest SiO_2 concentration (10.7 mM), the (100) diffraction peak is very broad and the (110) peak is absent. The TGA analysis (Fig. S3) suggests that the silica content in this film is around 16.4 wt% which is much lower than for the film prepared from 43.0 mM SiO_2 (30.2 wt%). We hypothesize that the low ordering may be due to the limited amount of silica available to form the silica scaffold around the CTAB-LPEI template which therefore restricts the packing of the adjacent micelles into a well-ordered structure. The highest silica concentration also results in a less ordered film using this method, possibly due to excess silica between the micelles hindering the ordering [48].

The (100) peak positions are slightly different as the silica concentration changes. Recalling that the relationship between the position of the peak and the *d* spacing (*d*) is:

$$d = \frac{2\pi}{Q} \qquad \text{Equation 1}$$

where *Q* is the position of the first peak, the calculated *d* spacings range between 39.3 and 41.6 Å, as listed in Table 1. More SiO_2 is expected to increase the wall thickness of the silica films, resulting in larger *d* spacings. However, sodium ions and hydroxide introduced along with SiO_2 also influence the formation of micelles and the interaction between templates and silica species. Therefore, the *d* spacing does not increase monotonically with the concentration of the SiO_2.

Our visual observation showed that the film formation time strongly depended on the concentration of the SiO_2. Therefore, we quantified the film formation time by monitoring surface pressure at the air/liquid interfaces in real-time. Measurements of the surface pressure started *ca.* 6 min after the solutions were mixed, and are plotted versus time as shown in Fig. 2A. In the first 5 min of measurement, the surface pressure shows a weak variation. Specifically, for the two lowest concentrations (21.7 and 32.3 mM), the surface pressure slightly increases above 0 mN/m; while it decreases to reach −0.5 mN/m for the other concentrations (between 43.0 and 86.3 mM). After this change at an early stage, the surface pressure remains constant until the film growth induced an apparent decrease of the surface pressure. However, when no silica is present, the growth of the CTAB-LPEI film induces an initial drop in surface pressure due to rapid film formation (within seconds) and attachment to the fibre, followed by a gradual increase in surface pressure with time to a plateau as the film grows in thickness thereafter [35]. This behaviour is also very different from that observed when TMOS is used as the silica source for preparing free-standing silica-CTAB films in acidic solutions. For TMOS containing systems, at early times, the surface pressure experiences a fall-off due to the lower surface tension of methanol saturating at the interface as the hydrolysis proceeds and the lower surface tension is also associated with a decrease in the height of the meniscus, caused by the evaporation of the methanol from the solution [41]. These suggest the initial surface pressure change observed in the current system has a close relation to the polymerization process of the silica precursor.

For the lowest concentration of SiO_2 (21.7 mM), the surface pressure gradually decreases from 29 min onwards; while for the other concentrations the decrease is found at later times and is more abrupt. We relate this apparent drop in surface pressure with the attachment of solid films on the fibre. Hence, the time associated with this decrease in surface pressure is defined as the time when the film solidified and is heavy enough to be detected, namely the initial film formation time (plotted in Fig. 2B). Rapid film formation happens when the SiO_2 concentration was relatively low. The initial film formation time increases with concentration until a maximum at *ca.* 50–60 mM, before decreasing for higher concentrations.

The polymerization process of the SiO_2 species in the alkaline solutions is here the key factor driving the film formation. In mildly alkaline aqueous solutions, silica species appear predominantly as $Si(OH)_4^0$ neutral species [46,47]. In our condition, where Na-silicate is added into highly alkaline solutions (pH > 10) [47], the oligomerization of the monomers (Eq. (1)) followed by deprotonation (Eq. (2)) and

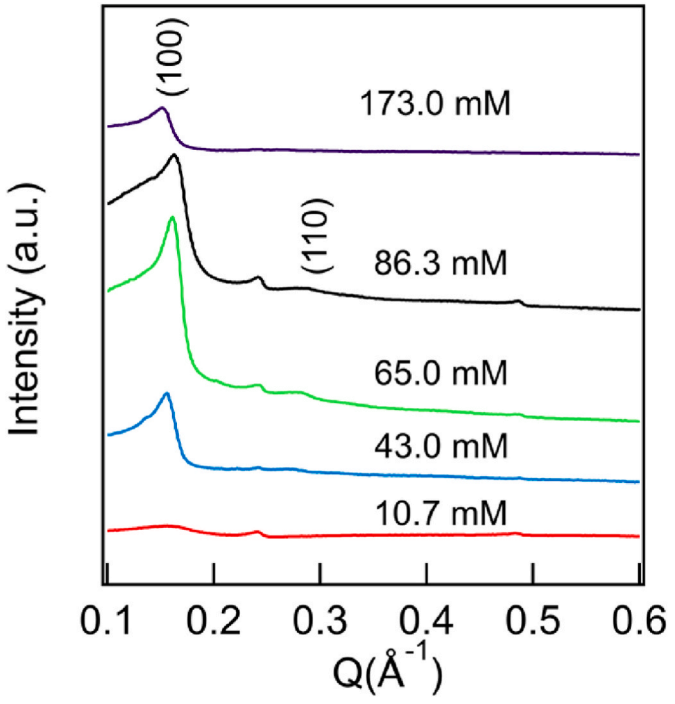

Fig. 1. SAXS patterns of as-prepared dry silica films synthesized from CTAB (37.0 mM)/LPEI (0.3 mM)/NaOH (100.0 mM) systems with varied SiO_2 concentrations. Normalized molar ratios of SiO_2: CTAB: LPEI are 1:0.21:0.002, 1:0.43:0.003, 1:0.57:0.005, 1:0.86:0.007 and 1:3.46:0.028 from top to bottom respectively.

Table 1
The (100) peak positions and corresponding d spacings of as-prepared dry silica films synthesized from CTAB (37.0 mM)/LPEI (0.3 mM)/NaOH (100.0 mM) systems with different SiO_2 concentrations.

Conc. of SiO_2/mM	(100) peak position/$Å^{-1}$	*d* spacing/Å
10.7	Too broad	–
43.0	0.155 ± 0.001	40.5 ±. 0.3
65.0	0.160 ± 0.001	39.3 ±. 0.2
86.3	0.162 ± 0.001	38.8 ± 0.2
173.0	0.151 ± 0.001	41.6 ± 0.3

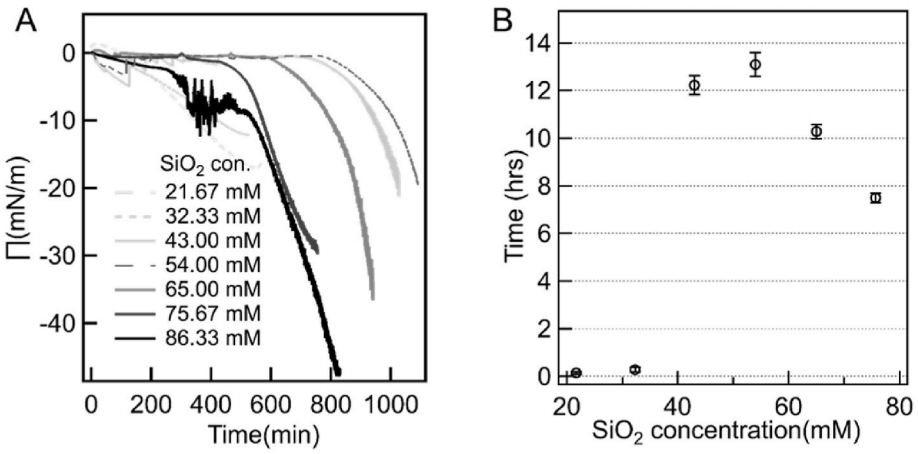

Fig. 2. (A) The changes in surface pressure with time. (B) Initial film formation time estimated from the surface pressure change. The concentration of SiO_2 was varied with CTAB, LPEI and NaOH concentration kept constant at 37.0, 0.3 and 100.0 mM, respectively, giving normalized molar ratios of SiO_2: CTAB: LPEI at 1:0.43:0.003, 1:0.48:0.004, 1:0.57:0.005, 1:0.69:0.006, 1:0.86:0.007, 1:1.15:0.009 and 1:1.71:0.14.

polycondensation reactions govern the aqueous equilibria [46,47, 49–51].

$$kSi(OH)_4^0 \rightleftharpoons \left[Si_kO_l(OH)_{4k-2l}\right]^0 + lH_2O, \quad 2 \le k \le 8 \tag{1}$$

where l denotes the number of the bridging oxygens (-Si-O-Si-).

the solution. At low SiO_2 concentrations, the silica species deprotonate and polymerize fast (Eq. (2)) and condense around the positively charged CTAB-LPEI templates thanks to electrostatic interactions, and these migrate to the interface to form silica films. When the Na-silicate content increases but with the same NaOH concentration in the solution, the completion of the deprotonation and polycondensation of silica

$$\left[Si_kO_l(OH)_{4k-2l}\right]^0 + mOH^- + mNa^+ \rightleftharpoons \left[Si_{nk}O_{n(l+m)}(OH)_{4k-2l-m}\right]^{m-} \cdot mNa^+ + mH_2O \tag{2}$$

where m is the number of singly-negatively charged oxygen anions. After that, the produced silica species (Eq. (2)) polymerize with a repetition of n, which also bear negative charges, attracting sodium ions and CTA^+ in

species require a longer time, slowing down film formation. Nonetheless, for the higher concentrations of SiO_2, the initial film formation time decreases again. This may be due to the higher silica oligomer to surfactant template ratio, which allows greater contact between silica

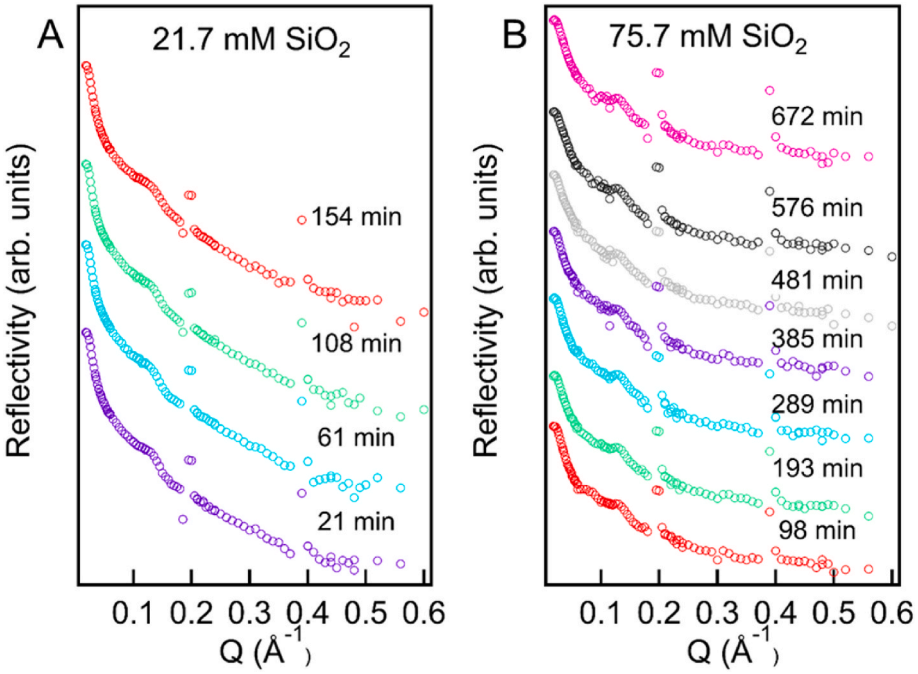

Fig. 3. In situ XRR curves taken while the films were forming at the surface with (A) 21.7 (SiO_2:CTAB:LPEI = 1:1.71:0.014) or (B) 75.7 mM (SiO_2:CTAB:LPEI = 1:0.48:0.004) SiO_2 concentrations. Patterns are offset vertically for clarity.

species and the template, and less electrostatic repulsion between more completely silica-coated cylindrical micelles to shield the charge on the micelles while packing [41,52]. These effects reduce the energy required for packing of the adjacent cylindrical micelles into a 2D hexagonal structure [53]. These changes consequently, are reflected as a drop in the initial film formation time.

The evolution of the surface structure was followed by XRR at different time intervals (times are labelled in figures) to try to determine whether the film formation event measured by surface tension was related to the mesostructure in the film. The intensity of the reflected X-ray beam is due to the large contrast of electron densities between the CTAB-LPEI template and the silica matrix. At early stages, the XRR patterns are similar for solutions with different SiO_2 concentrations; a broad peak at around 0.125 $Å^{-1}$ and two sharp peaks at 0.195 and 0.390 $Å^{-1}$, respectively. The two sharp peaks are assigned to excess CTAB surfactant crystals in a hydrated state [54,55]. The broad peak is related to a wormlike structure formed at the interface [56,57], which has already formed at an early stage of the reaction when no visible film is present at the interface.

However the XRR pattern did not vary significantly with time over the period measured (see Fig. 3 and Fig. S4), even after the initial film formation time found in the surface pressure measurements. The peak appearing at Q = 0.125 $Å^{-1}$ in XRR the patterns corresponds to the (100) diffraction peak at higher Q (0.160 $Å^{-1}$) observed in the SAXS pattern of the dry film, indicating a shrinkage of structure with the d spacing changing from 50.24 Å to 39.25 Å due to the solvent evaporation and silica condensation upon drying. However, the (110) peak that appears in the SAXS patterns of the dry silica films is not found in the XRR patterns. Three scenarios can explain this absence: the 2D hexagonal phase is aligned with the long axis of the micelles parallel to the solution interface, so that the (110) peak does not intersect with the detector in the reflection geometry [58]; if the 2D hexagonal phase in the film is not aligned but is composed of multiple crystallites with random orientation then the (110) Bragg peak (which is assumed to be found at Q_{110} = 0.220 $Å^{-1}$) could be hidden by the sharp peak associated with the crystalline surfactant at 0.195 $Å^{-1}$; or the film experiences a reorganization from a wormlike structure into a 2D-hexagonal one during drying. In previous work on surfactant templated silica films grown at the air-solution interface, the high degree of orientation of the well-ordered 2D hexagonal phase near the interface means that the (110) is not typically seen in the XRR data [58], however, it can be identified in the in-plane scattering measured via GISAXS [59,60].

The film growth and ordering of these CTAB-LPEI-silica films were therefore observed via the GISAXS patterns to determine whether the film organization is truly 2D hexagonal or more disordered. As displayed in Fig. 4, the GISAXS pattern (collected at 70 min after the reaction started, for a solution with a SiO_2 concentration at 65.0 mM), as a representative example, contains three diffraction features. First, two

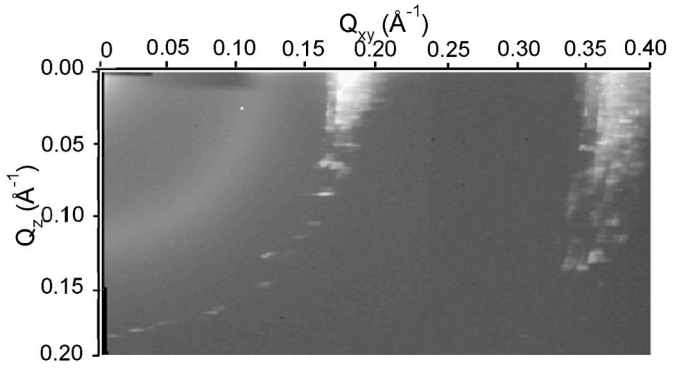

Fig. 4. GISAXS pattern of the film formed at 70 min with a SiO_2 concentration at 75.7 mM (SiO_2: CTAB: LPEI = 1:0.86:0.007), collected just after the first XRR pattern in Fig. 3B with an incident angle of 0.1°.

broad but preferentially oriented peaks at around Q_z = 0.190 and 0.380 $Å^{-1}$ are correlated to the sharp reflection peaks at 0.195 and 0.390 $Å^{-1}$ in the XRR data and hence associated with the crystallisation of the surfactant. The GISAXS data also contains an isotropic ring crossing Q_{xy} and Q_z at around 0.125 $Å^{-1}$, but no peak at the expected position of the (110), indicating the formation of wormlike mesostructures with no preferential orientation at the interface [61]. The GISAXS patterns of films grown from solutions at other Na-silicate concentrations are shown in Fig. S5 where surfactant crystallisation and wormlike film structures are also observed. We therefore conclude that the 2D hexagonal ordering of the dry films must occur as a result of continuing silica condensation and water loss after removal from the air-solution interface.

3.2. Effects of the concentration of NaOH, CTAB and LPEI on CTAB-LPEI-silica films

The other relevant experimental parameters controlling film growth, the concentrations of NaOH, CTAB and LPEI in the solution, were also investigated, but had less significant effects on film formation than the silica concentration so are briefly described. NaOH controls the pH of the solution, without which films are not able to form. The concentrations of NaOH investigated were 25.0, 50.0, 75.0 and 100.0 mM, giving a pH range between 12.3 and 12.8. SAXS patterns of the dried as-prepared films (Fig. 5A) possess three peaks, assigned to the (100) and (110) diffraction peaks of the 2D hexagonal structure plus a sharper peak at 0.24 $Å^{-1}$ due to crystalline surfactant. The positions of the primary peaks and corresponding *d* spacings are listed in Table S1 and are all around 40 Å. Neither the *d* spacings nor the intensity of the peak varies significantly with the NaOH concentration of the film formation solution. The third peak which can be indexed to the (110) Bragg peak is observed in these SAXS patterns, confirming the periodically ordered structure [61]. To explain the small differences in the mesostructure of the prepared silica films obtained, both the LPEI and Na-silicate solution are alkaline and thus the variation of NaOH content only allows a narrow range of the pH to be explored (12.3–12.8), resulting in an insignificant structural difference in the mesostructured silica materials produced.

The concentration of CTAB, as the main part of the soft template, was also varied from 14.8 mM to 37.0 mM. The intensity of the first peak becomes less distinct as the concentration of CTAB increases (refer to Fig. 5B), which demonstrates a reduction of the ordering in the dry silica film. The *d* spacing of the prepared films are listed in Table S1, but again little variation in peak position is observed. Adjusting CTAB concentration also changes the template ratio between CTAB and LPEI (with a molar ratio of 123:1, 98:1, 74:1 and 50:1), therefore, affects the structure of the resulting films. A lower CTAB:LPEI ratio is conducive to the growth of the (100) peak, while a higher CTAB:LPEI ratio in the solution produces materials where the (110) peak intensity is higher relative to the (100) peak intensity.

The effect of LPEI concentration, as a co-templating component, was studied in a SiO_2 (43.0 mM)/CTAB (37.0 mM) system. As the LPEI concentration increases, peaks in SAXS patterns have small differences in intensity (Fig. 5C) and the peak positions are similar, as reported in Table S1.

3.3. Effect of the addition of $NaNO_3$ on CTAB-LPEI-silica films

Although thick films were formed using CTAB-LPEI-silica solutions, variation of the synthesis parameters did not greatly improve mesostructural ordering in the films, so a method to improve the self-organisation was sought. Adding nitrate ions was studied previously to induce the growth of CTAB micelles in water and so improve their effect on the ordering of templated mesostructured inorganic materials [62–64]. Herein, $NaNO_3$ was chosen as a source of nitrate ions, to study the effect of NO_3^- on the structure of the silica films formed at the

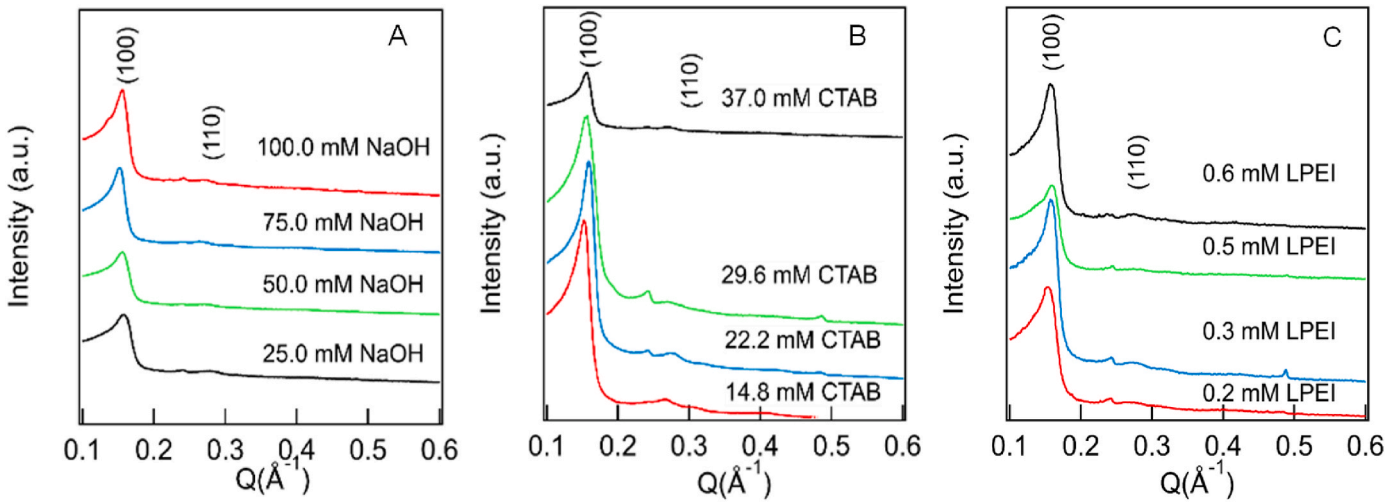

Fig. 5. The SAXS patterns of as-prepared dry silica films synthesized from (A) SiO_2 (43.0 mM)\CTAB (37.0 mM)\LPEI (0.3 mM) systems (fixed SiO_2: CTAB: LPEI = 1:0.86:0.007) with different NaOH concentrations. (B) SiO_2 (43.0 mM)/LPEI (0.3 mM) systems with different CTAB concentrations, giving normalized molar ratio of SiO_2: CTAB: LPEI (from to bottom) at 1:(0.86, 0.67, 0.52, 0.34):0.07. (C) SiO_2 (43.0 mM)/CTAB (37.0 mM) systems with different LPEI concentrations, giving normalized molar ratio of SiO_2: CTAB: LPEI (from to bottom) at 1:0.86:(0.014, 0.012, 0.007, 0.005), respectively.

interface. In addition to the expected change in the ionic strength, NO_3^- is also known to associate with CTA^+ micelles much more strongly than Br^-. A fraction of the Br^- ions are replaced by NO_3^- at the micelle solvent interfaces [63], screening charge on the CTA^+ headgroups, and causing elongated micelles to form in solution, while in general the addition of monovalent salts, also causes the solubility of ionic surfactants to decrease. The effect of NO_3^-, up to a concentration of 74.0 mM, was studied at fixed CTAB (37.0 mM), LPEI (0.3 mM) and NaOH (100.0 mM) concentrations.

The real-time surface pressure measurements indicate a doubling of the initial film formation time (450 min versus 220 min) when 25.0 mM $NaNO_3$ is present in the solution (Fig. S6). This corresponds to the longer formation time required for CTAB-LPEI free-standing films when salt is present, previously reported by Edler and co-workers [32], possibly due to the enhanced charge screening and maybe also because of the higher solution viscosity, arising due to the elongated micelles, that hinders the diffusion of species to the interface.

The addition of 25.0 mM $NaNO_3$ allowed a more even film to form, with no crystalline surfactant observed, as seen in Fig. S7. Moreover, the as-prepared dry film is thicker than a similar film prepared from a solution without added $NaNO_3$ (0.162 mm compared to 0.142 mm, measured by a digital calliper), and no precipitation of silica was observed in the petri dish. The clear and robust film prepared from solution containing 25.0 mM $NaNO_3$ was easily harvested from the interface and could be kept in one piece until drying. Cracks occurred after drying and the film became white rather than transparent. TGA results (Fig. S8) suggests a decrease in the weight percentage of the silica incorporated in the film from 24.6 wt% to 17.6 wt% when 25.0 mM $NaNO_3$ is present. Therefore, the addition of $NaNO_3$ induces formation of a thicker film with a higher template content, but a lower amount of silica, presumably due to the nitrate anion replacing silicate anions in binding to the micelle surface.

Comparing the SAXS patterns in Fig. 6A, the primary peak fades with increasing $NaNO_3$ concentration and vanishes when the concentration reaches 74.0 mM as the ionic screening effects outweigh any structural enhancement due to micelle elongation.

The slow fade of the (100) diffraction peak with increasing $NaNO_3$ concentration may be explained by the order of affinity toward the CTA^+ micelles reported: $OH^- < Cl^- < B_4O_7^{2-} < Br^- < NO_3^-$ [65]. The bidentate ligand $B_4O_7^{2-}$ in the sequence is reminiscent of oligomeric

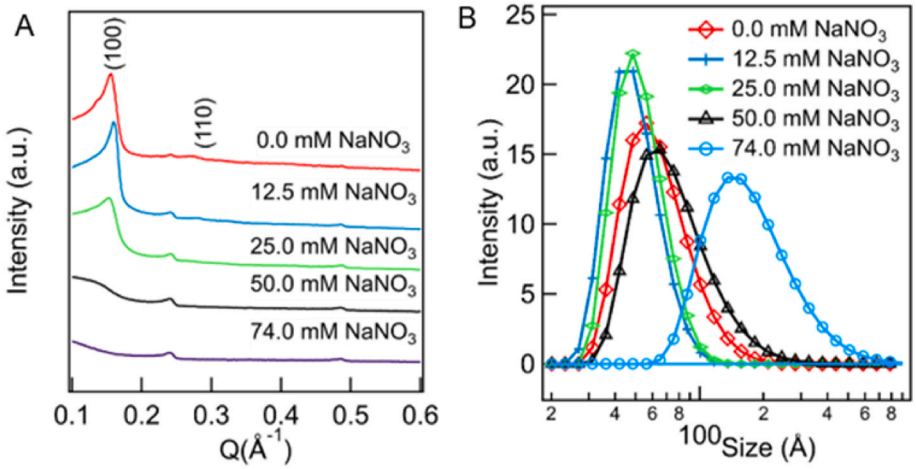

Fig. 6. (A) SAXS patterns of silica films prepared from SiO_2 (65.0 mM)/NaOH (100.0 mM)/CTAB (37.0 mM)/LPEI (0.3 mM) systems (fixed SiO_2: CTAB: LPEI = 1:0.57:0.005), with changing $NaNO_3$ concentration. (B) The volume-weighted size distribution of CTA^+ micelles in the presence of different $NaNO_3$ concentrations obtained in DLS (CTAB concentration 37.0 mM) and treated via the CONTIN analysis method.

silicates [66]. Therefore, the nitrate ions could bind more strongly at cationic micelle surfaces than the other species in our system (oligomeric silicate and Br^-) [67–69] so exchange for the Br^- on CTA^+ micelles [70]. This anion exchange may decrease the equilibrium area per molecule (a_0) of the CTA^+ headgroup due to the tighter binding of NO_3^- to the micellar surface. This gives a larger packing parameter, $g = v/a_0 l_c$ (v is the surfactant tail volume, a_0 is the equilibrium area per molecule and l_c is the tail length) [71], causing the elongation of the micelles and may further increase the viscosity of the solution if the degree of elongation is large enough [69,70].

The highest concentration of $NaNO_3$ we studied here is sufficiently large (74.0 mM, twice the concentration of CTAB) to replace most of the Br^- ions in CTAB. The resulting solution is of high viscosity [69] due to the elongation and the crosslinking of the micelles, causing a slow flow of the template micelles from the bulk to the interface to form films. Therefore, the film harvested is poorly ordered. To corroborate this, 37.0 mM CTAB solutions in the presence of different $NaNO_3$ concentrations were studied using dynamic light scattering (DLS) and data were treated using the CONTIN method. Although the CONTIN analysis assumes a spherical shape for the particles probed, the trends in the data confirm micellar growth. As plotted in Fig. 6B, when the concentration of $NaNO_3$ is low (at 12.5 and 25.0 mM), DLS results give slightly smaller averaged micellar sizes due to the screening effect caused by the introduced ions. A size growth of micelles is detected using DLS at higher $NaNO_3$ concentrations. Then a dramatic increase in size is observed at the highest concentration (74.0 mM) we studied. Unfortunately, the opaque solutions generated when Na-silicate is added to the CTAB/L-PEI/$NaNO_3$ solutions prevent the observation of the effect of adding silicate anion on micellar size using this method.

The (100) reflected peak in the *in situ* XRR patterns from solutions containing SiO_2/CTAB/LPEI/$NaNO_3$, as displayed in Fig. 7, stays at around 0.125 $Å^{-1}$. This suggests the ions have little effect on the *d* spacing of micelle structure normal to the surface. Moreover, no sharp reflected peaks from crystalline surfactant are observed in presence of $NaNO_3$, indicating that more surfactant remained soluble and so has the chance to contribute to film formation in the presence of NO_3^-. This collaborates with the TGA results (see Fig. S8), which show that the film prepared has a higher content of organic template. A broad secondary reflected peak is also seen in the reflectivity patterns (ca. 0.190 $Å^{-1}$) at the end of the measurements for $NaNO_3$ concentrations of 12.5 and 25.0 mM (Fig. 7A and B), giving evidence of the formation of a wormlike disordered structure along the perpendicular direction to the surface. However, the rise of the secondary peak is not seen at 50.0 mM $NaNO_3$ (Fig. 7C), which may be due to the relatively high viscosity of this solution hindering micelle packing in the films.

We can also see the reduction of crystallised surfactant in GISAXS patterns (Fig. 8). There are two rings in the GISAXS patterns associated with the film formation solution in the presence of 12.5 mM $NaNO_3$ (Fig. 8A), of which one crosses both the y and z axes at 0.125 $Å^{-1}$, corresponding to a characteristic period of 50.2 ± 5.0 Å. There is also a relatively indistinct ring which is related to the crystalline surfactant structure comparable to the one in Fig. 4, however, this is not observed in the corresponding XRR patterns (Fig. 7A) which may be due to the low intensity. With elevated $NaNO_3$ concentrations (25.0 mM and 50.0 mM), this ring, due to the crystallised surfactants, disappears still further, leaving a single ring which related to the wormlike structure in these GISAXS patterns (Fig. 8B and C). Moreover, the centre of the broad ring moves progressively closer to the beam centre when more $NaNO_3$ is present. This suggests a larger *d* spacing, which is related to a higher amount of the templating species in the films; the charged micelles are not completely neutralised by the oligomeric silicates in between the micelles; electrostatic repulsion between the charged micelles therefore increases their spacing within the films. Similarly, this effect is seen for CTAB-SPEI (polyethylenimine, Mw *ca.* 2000 Da) films in the absence of silica where added salt (NaBr) resulted in an increase in the *d* spacing within the films (Fig. S9).

No (110) peaks are seen in the GISAXS patterns at the end of the measurements, as seen in Fig. 9. Thus although addition of NO_3^- anions did not achieve the intended improvement of mesostructural ordering in the films, the combination of XRR and GISAXS results, in the presence and absence of NO_3^- anions, leads us to suggest a possible formation process of the film: the elongated micelles form initially in the solution at an early stage, then a solid film with wormlike structure is formed at the solution interface due to the combination of solvent flux driving the

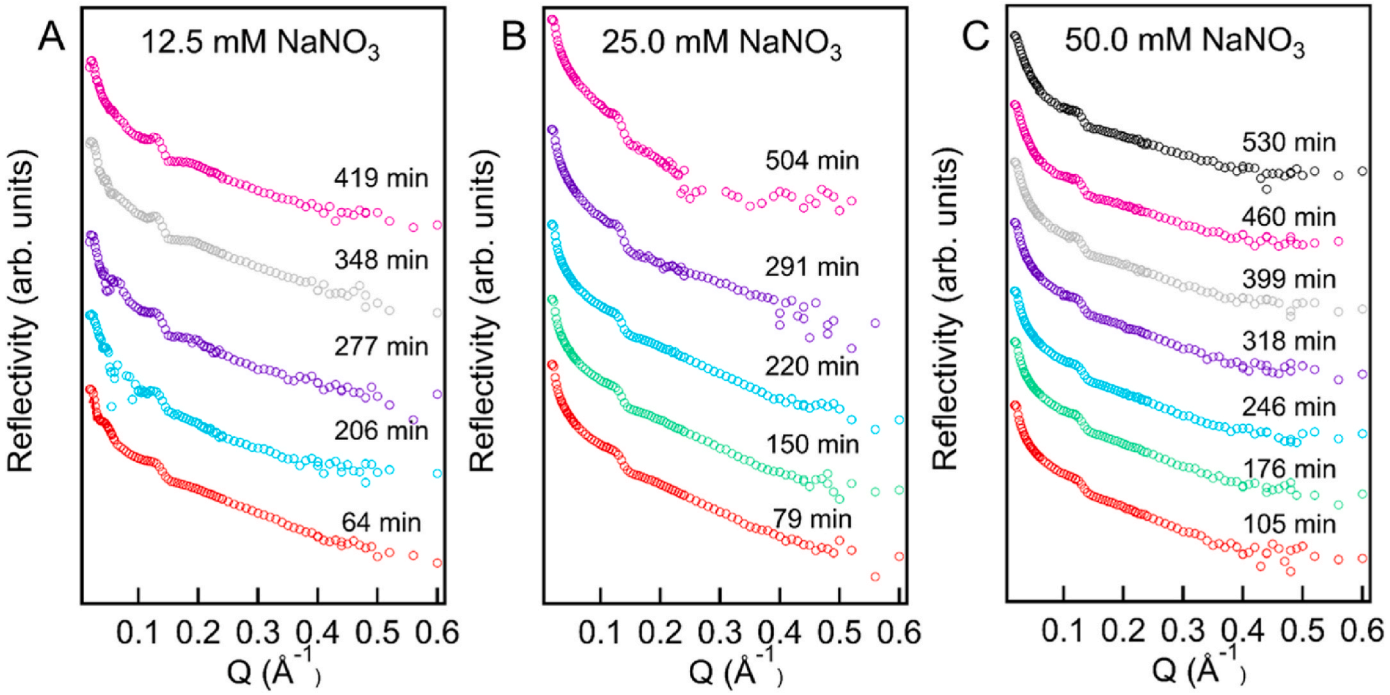

Fig. 7. In situ XRR curves taken while the films were forming at the surface with $NaNO_3$ concentration at (A) 12.5, (B) 25.0 and (C) 50.0 mM with fixed SiO_2 (65.0 mM), CTAB (37.0 mM), LPEI (0.3 mM) and NaOH (100.0 mM) concentrations.

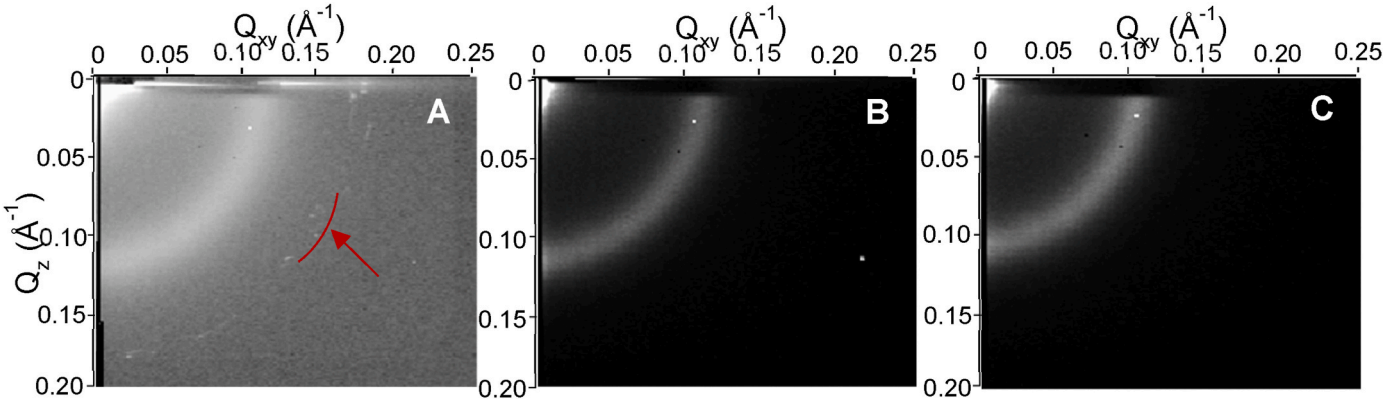

Fig. 8. GISAXS patterns of the structure of the interface at an incident angle of 0.1° at the early stage of the film formation in the presence of (A) 12.5 mM $NaNO_3$ (B) 25.0 mM $NaNO_3$ (C) 50.0 mM $NaNO_3$ with fixed SiO_2 (65.0 mM), CTAB (37.0 mM), LPEI (0.3 mM) and NaOH (100.0 mM) concentrations. The arrow in Fig. 8A indicates a ring which is the reflection peak from crystaline surfactant.

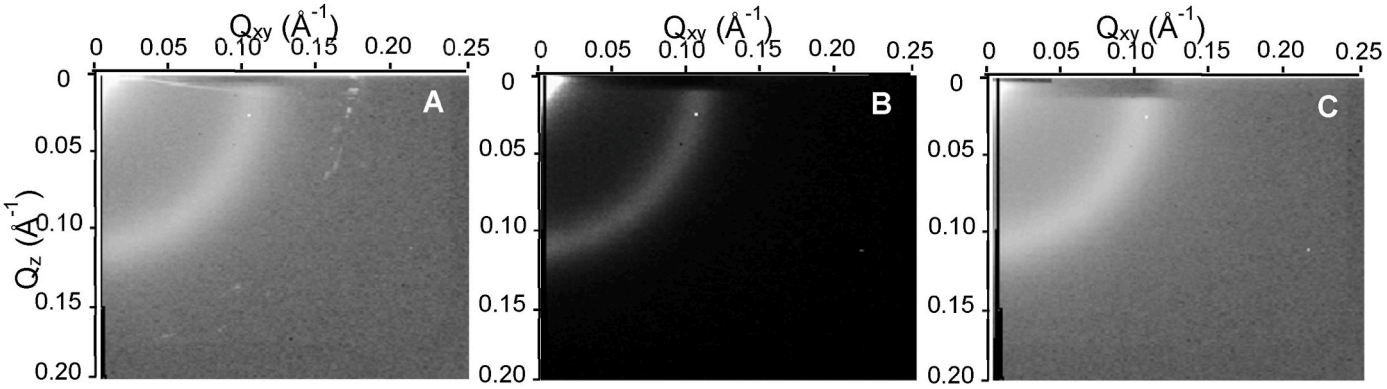

Fig. 9. GISAXS patterns of the structure of the interface at an incident angle of 0.1° at the end of the film formation in the presence of (A) 12.5 mM $NaNO_3$ (B) 25.0 mM $NaNO_3$ (C) 50.0 mM $NaNO_3$ with fixed SiO_2 (65.0 mM), CTAB (37.0 mM), LPEI (0.3 mM) and NaOH (100.0 mM) concentrations.

micelles to the interface and the lowering of the interface as the solvent gradually evaporates [72]. After removal from the interface, while more solvent is evaporating, the elongated micelles become more concentrated which drives further ordering, causing them to hexagonally pack within the film. A 2D hexagonal structure with random orientation forms the bulk of the film and so is observed in the transmission SAXS patterns after the films are dried.

3.4. Removal of CTAB-LPEI template

The organic template was removed by calcination in air to obtain porous films. The film grown from a solution containing 25.0 mM $NaNO_3$ was dried and calcined without and with pre-treatments described in the experimental section (washing and pre-calcination as described in the experimental section above). When the dried film was calcined directly at 600 °C, the flat SAXS pattern (Fig. 10A, curve b) suggests the mesostructure completely collapses; the NaOH in the film becomes concentrated during calcination and destroys the mesostructure set by the silica. With pre-treatments, a relatively poor long-range order is retained as illustrated by a broad diffraction peak in the SAXS pattern (Fig. 10A, curve c). A photograph of small pieces of calcined film are given in Fig. S10. SEM images of the silica film before and after calcination, as illustrated in Fig. 10B and (C), show a homogeneous and continuous morphology of silica. Sample a has a low BET surface area of *ca.* 15.5 m^2/g due to the blocking of the pores by the CTAB and LPEI molecules prior to calcination. The nitrogen sorption isotherm (Fig. 10D) of sample c is a type IV isotherm with a type H4 hysteresis loop [73,74] and gives a surface area of 660.4 $m^2\ g^{-1}$ obtained using the BET method. The pore size is distributed between 1 nm and 10 nm with most of the pores under 5 nm (the inset of Fig. 10D). Therefore, the pre-treatment strategy provides a mild way to remove alkaline content from the film using water and strengthen the mesostructure formed by silica through pre-calcination.

4. Conclusion

Na-silicate, an environmentally friendly and cheap silica source, was used to synthesize mesostructured silica films at the air/solution interface using a CTAB/LPEI template from alkaline solutions. Using Na-silicate allows the formation of free-standing composite films containing a 2D hexagonal mesostructure over a wide composition range, without producing any alcohol during condensation compared to silicon alkoxides. Variation of the CTAB, LPEI and pH did not strongly affect film structures, but silica concentration in solution directly affected silica incorporation into the film and the degree of mesostructural ordering in the dry films. The *in situ* GISAXS and XRR results show an intense reflection from crystallised surfactant at the interface in addition to a broad peak related to the templated silica. The introduction of 25.0 mM $NaNO_3$ to the system effectively prevents the surfactant species from crystallising and also forms a thicker film but prolongs the initial film formation time. *In situ* GISAXS and XRR suggest the surface layer has a wormlike liquid crystalline structure. The 2D hexagonal structure forms while the films are drying at room temperature. Water washing and pre-calcination before calcination of the films protect the mesostructure from collapsing to some extent, however the calcined silica films have relatively a poor long-range order compared to the ambient

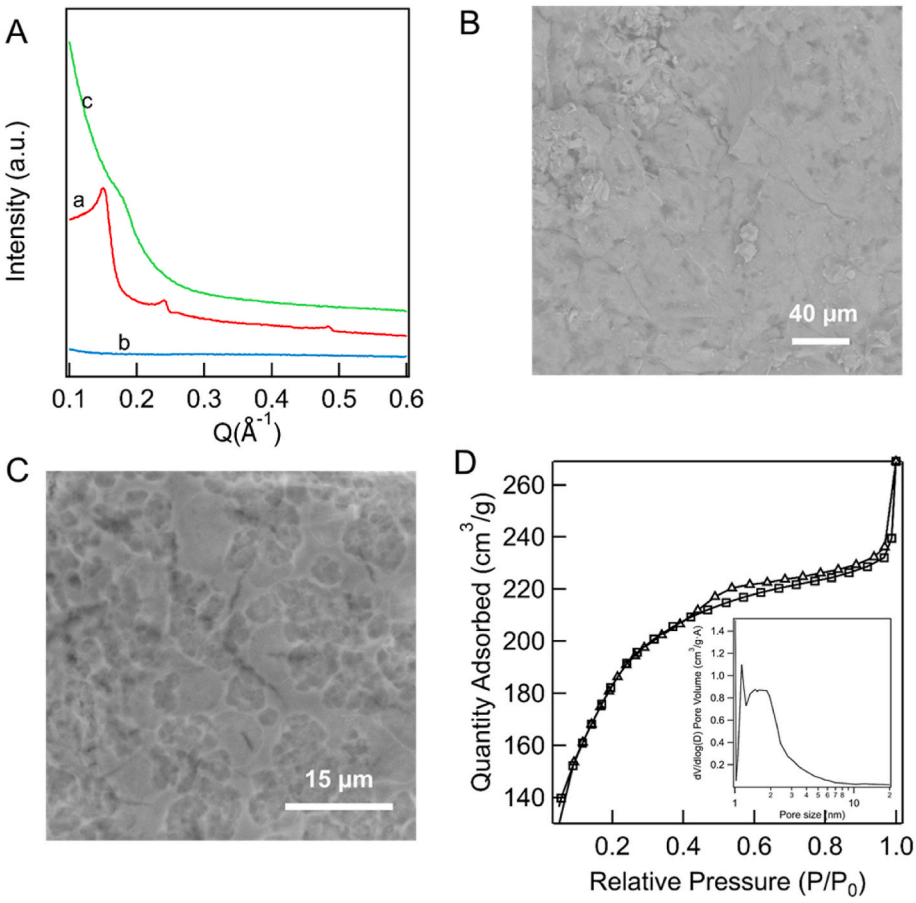

Fig. 10. (A) SAXS patterns of films grown from CTAB (37.0 mM)/LPEI (0.3 mM)/NaOH (100.0 mM)/SiO_2 (65.0 mM)/$NaNO_3$ (25.0 mM) solution. (a) The as-prepared dry film. (b) The calcined film without pre-treatment and (c) with pre-treatment. SEM images of (B) as-prepared dry film and (C) calcined silica film with pre-treatment. (D) Nitrogen sorption isotherm for sample c in Fig.10A. The inset is the pore size distribution of sample c, obtained from BJH analysis [75].

dried silica films containing the template, although they remain as continuous membranes and present a relatively high surface area of *ca.* 660.4 m^2/g.

Although this preparation method could not maintain the ordering of the mesostructure, it provides a way to encapsulate materials (nanomaterials or biomaterials) that are only stable in alkaline conditions into free-standing silica films. The films prepared are thicker than those typically accessible by EISA and EASA methods and the film morphology is maintained during calcination. Na-silicate solution is a cheaper silica source than alkoxysilanes and also avoids the presence of alcohols during the film synthesis, which can affect both self-assembly of the surfactant mesophase and potential encapsulated species. In addition, this method allows the *in situ* inspection of the encapsulation process at the interface, which could contribute to the investigation of mesophase evolution during the encapsulation process and interactions between species during incorporation within the film at the interface.

CRediT authorship contribution statement

Andi Di: Writing – original draft, Methodology, Investigation, Formal analysis, Data curation, Conceptualization, Writing – review & editing. **Julien Schmitt:** Formal analysis, Investigation, Writing – review & editing. **Naomi Elstone:** Methodology, Investigation. **Thomas Arnold:** Conceptualization, Investigation, Methodology, Supervision, Writing – review & editing. **Karen J. Edler:** Writing – review & editing, Supervision, Resources, Project administration, Methodology, Funding acquisition, Data curation, Conceptualization.

Declaration of competing interest

The authors declare that they have no known competing financial interests or personal relationships that could have appeared to influence the work reported in this paper.

Acknowledgements

A. Di would like to thank the China Scholarship Council and the University of Bath for funding her PhD studies. N. Elstone thanks the UK Engineering and Physical Sciences Research Council (EPSRC), for a PhD studentship in the Centre for Doctoral Training in Sustainable Chemical Technologies at the University of Bath (EP/L016354/1). The authors thank Diamond Light Source (UK) for the award of beamtime on beamline I07 (experiment SI52101-1), and the ISIS Neutron and Muon Source for beamtime on CRISP (DOI: 10.5286/ISIS.E.RB13425). The authors would like to acknowledge Dr Johnathan Rawle for his assistance with the reduction of GISAXS data and Dr Stephen Holt for assistance with the experiment on CRISP. Data supporting this paper are available through the University of Bath research data archive system, DOI: https://doi.org/10.15125/BATH-01151.

Appendix A. Supplementary data

Supplementary data to this article can be found online at https://doi.org/10.1016/j.micromeso.2022.112018.

References

[1] T.-L. Chew, A.L. Ahmad, S. Bhatia, Ordered mesoporous silica (OMS) as an adsorbent and membrane for separation of carbon dioxide (CO2), Adv. Colloid Interface Sci. 153 (2010) 43–57.
[2] B. Zornoza, C. Téllez, J. Coronas, Mixed matrix membranes comprising glassy polymers and dispersed mesoporous silica spheres for gas separation, J. Membr. Sci. 368 (2011) 100–109.
[3] T. Maschmeyer, F. Rey, G. Sankar, J.M. Thomas, Heterogeneous catalysts obtained by grafting metallocene complexes onto mesoporous silica, Nature 378 (1995) 159–162.
[4] F. Jiao, H. Frei, Nanostructured cobalt oxide clusters in mesoporous silica as efficient oxygen-evolving catalysts, Angew. Chem. Int. Ed. 48 (2009) 1841–1844.
[5] X. Li, Y. Yang, Q. Yang, Organo-functionalized silica hollow nanospheres: synthesis and catalytic application, J. Mater. Chem. 1 (2013) 1525–1535.
[6] P.C. Angelomé, et al., Growth and branching of gold nanoparticles through mesoporous silica thin films, Nanoscale 4 (2012) 931–939.
[7] C.T. Kresge, M.E. Leonowicz, W.J. Roth, J.C. Vartuli, J.S. Beck, Ordered mesoporous molecular sieves synthesized by a liquid-crystal template mechanism, Nature 359 (1992) 710.
[8] S. Che, et al., Synthesis and characterization of chiral mesoporous silica, Nature 429 (2004) 281.
[9] D. Grosso, et al., Two-dimensional hexagonal mesoporous silica thin films prepared from block copolymers: detailed characterization and formation mechanism, Chem. Mater. 13 (2001) 1848–1856.
[10] J. Patarin, B. Lebeau, R. Zana, Recent advances in the formation mechanisms of organized mesoporous materials, Curr. Opin. Colloid Interface Sci. 7 (2002) 107–115.
[11] M. Kruk, M. Jaroniec, C.H. Ko, R. Ryoo, Characterization of the porous structure of SBA-15, Chem. Mater. 12 (2000) 1961–1968.
[12] Y. Zhou, J.H. Schattka, M. Antonietti, Room-temperature ionic liquids as template to monolithic mesoporous silica with wormlike pores via a sol- gel nanocasting technique, Nano Lett. 4 (2004) 477–481.
[13] D. Zhao, et al., Triblock copolymer syntheses of mesoporous silica with periodic 50 to 300 angstrom pores, Science 279 (1998) 548–552 (80-.).
[14] P. Yang, D. Zhao, B.F. Chmelka, G.D. Stucky, Triblock-copolymer-directed syntheses of large-pore mesoporous silica fibers, Chem. Mater. 10 (1998) 2033–2036.
[15] K. Chao, P. Liu, K. Huang, Thin films of mesoporous silica: characterization and applications, Compt. Rendus Chem. 8 (2005) 727–739.
[16] L. Nicole, C. Boissière, D. Grosso, A. Quach, C. Sanchez, Mesostructured hybrid organic-inorganic thin films, J. Mater. Chem. 15 (2005) 3598–3627.
[17] B.A. McCool, N. Hill, J. DiCarlo, W.J. DeSisto, Synthesis and characterization of mesoporous silica membranes via dip-coating and hydrothermal deposition techniques, J. Membr. Sci. 218 (2003) 55–67.
[18] X. Lin, Q. Yang, L. Ding, B. Su, Ultrathin silica membranes with highly ordered and perpendicular nanochannels for precise and fast molecular separation, ACS Nano 9 (2015) 11266–11277.
[19] Y. Ye, C. Jo, I. Jeong, J. Lee, Functional mesoporous materials for energy applications: solar cells, fuel cells, and batteries, Nanoscale 5 (2013) 4584–4605.
[20] P.B. Sarawade, G.N. Shao, D.V. Quang, H.T. Kim, Effect of various structure directing agents on the physicochemical properties of the silica aerogels prepared at an ambient pressure, Appl. Surf. Sci. 287 (2013) 84–90.
[21] D. Zhao, et al., Continuous mesoporous silica films with highly ordered large pore structures, Adv. Mater. 10 (1998) 1380–1385.
[22] A. Mitra, C. Vázquez-Vázquez, M.A. López-Quintela, B.K. Paul, A. Bhaumik, Soft-templating approach for the synthesis of high surface area and superparamagnetic mesoporous iron oxide materials, Microporous Mesoporous Mater. 131 (2010) 373–377.
[23] A. Walcarius, E. Sibottier, M. Etienne, J. Ghanbaja, Electrochemically assisted self-assembly of mesoporous silica thin films, Nat. Mater. 6 (2007) 602.
[24] A. Goux, et al., Oriented mesoporous silica films obtained by electro-assisted self-assembly (EASA), Chem. Mater. 21 (2009) 731–741.
[25] A. Gibaud, et al., Evaporation-controlled self-assembly of silica surfactant mesophases, J. Phys. Chem. B 107 (2003) 6114–6118.
[26] Y. Lu, et al., Continuous formation of supported cubic and hexagonal mesoporous films by sol-gel dip-coating, Nature 389 (1997) 364.
[27] N. Nishiyama, S. Tanaka, Y. Egashira, Y. Oku, K. Ueyama, Enhancement of structural stability of mesoporous silica thin films prepared by spin-coating, Chem. Mater. 14 (2002) 4229–4234.
[28] J. Lee, et al., Characterization of mesoporous silica thin films for application to thermal isolation layer, Thin Solid Films 660 (2018) 715–719.
[29] H. Yang, N. Coombs, I. Sokolov, G.A. Ozin, Free-standing and oriented mesoporous silica films grown at the air-water interface, Nature 381 (1996) 589.
[30] K.J. Edler, S.J. Roser, Growth and characterization of mesoporous silica films, Int. Rev. Phys. Chem. 20 (2001) 387–466.
[31] B. Yang, J.A. Holdaway, K.J. Edler, Robust ordered cubic mesostructured polymer/silica composite films grown at the air/water interface, Langmuir 29 (2013) 4148–4158.
[32] K.J. Edler, A. Goldar, T. Brennan, S.J. Roser, Spontaneous free-standing nanostructured film growth in polyelectrolyte-surfactant systems, Chem. Commun. (2003) 1724–1725.
[33] R.V. Klitzing, B. Kolaric, Foam films stabilized by poly (ethylene imine), Tenside Surfactants Deterg. 39 (2002) 247–253.
[34] D.B. Kudryavtsev, R.F. Bakeeva, L.A. Kudryavtseva, L.Y. Zakharova, V.F. Sopin, The catalytic effect of the cationic surfactant-polyethylene imine-water system in the hydrolysis ofO-alkylO-p-nitrophenyl chloromethylphosphonates, Russ. Chem. Bull. 49 (2000) 1501–1505.
[35] B.M.D. O'Driscoll, et al., Thin films of polyethylenimine and alkyltrimethylammonium bromides at the air/water interface, Macromolecules 38 (2005) 8785–8794.
[36] B.M.D. O'Driscoll, et al., Macroscopic, mesostructured cationic surfactant/neutral polymer films: structure and cross-linking, Langmuir 23 (2007) 4589–4598.
[37] B. Yang, K.J. Edler, Free-standing ordered mesoporous silica films synthesized with surfactant-polyelectrolyte complexes at the air/water interface, Chem. Mater. 21 (2009) 1221–1231.
[38] K.J. Edler, M.J. Wasbrough, J.A. Holdaway, B.M.D. O'Driscoll, Self-assembled films formed at the air-water interface from CTAB/SDS mixtures with water-soluble polymers, Langmuir 25 (2008) 4047–4055.
[39] G.B. Kolesar, W.H. Siddiqui, R.G. Geil, R.M. Malczewski, E.J. Hobbs, Subchronic inhalation toxicity of tetramethoxysilane in rats, Toxicology 13 (1989) 285–295.
[40] I.A. Alksay, M. Trau, Biomimetric pathways for assembling inorganic thin films, Science 273 (1996) 892 (80-.).
[41] K.J. Edler, T. Brennan, S.J. Roser, S. Mann, R.M. Richardson, Formation of CTAB-templated mesophase silicate films from acidic solutions, Microporous Mesoporous Mater. 62 (2003) 165–175.
[42] T. Arnold, et al., Implementation of a beam deflection system for studies of liquid interfaces on beamline I07 at Diamond, J. Synchrotron Radiat. 19 (2012) 408–416.
[43] C. Nicklin, T. Arnold, J. Rawle, A. Warne, Diamond beamline I07: a beamline for surface and interface diffraction, J. Synchrotron Radiat. 23 (2016) 1245–1253.
[44] M. Basham, et al., Data analysis workbench (DAWN), J. Synchrotron Radiat. 22 (2015) 853–858.
[45] J.R. Levine, J.B. Cohen, Y.W. Chung, P. Georgopoulos, Grazing-incidence small-angle X-ray scattering: new tool for studying thin film growth, J. Appl. Crystallogr. 22 (1989) 528–532.
[46] C.F. Baes, R.E. Mesmer, The Hydrolysis of Cations, John Wiley & Sons, New York, 1976.
[47] J. Šefčík, A.V. McCormick, Thermochemistry of aqueous silicate solution precursors to ceramics, AIChE J. 43 (1997) 2773–2784.
[48] P. Holmqvist, P. Alexandridis, B. Lindman, Modification of the microstructure in block copolymer- water-"oil" systems by varying the copolymer composition and the "oil" type: small-angle X-ray scattering and deuterium-NMR investigation, J. Phys. Chem. B 102 (1998) 1149–1158.
[49] C.T.G. Knight, R.J. Balec, S.D. Kinrade, The structure of silicate anions in aqueous alkaline solutions, Angew. Chem. Int. Ed. 46 (2007) 8148–8152.
[50] J.L. Bass, G.L. Turner, Anion distributions in sodium silicate solutions. Characterization by 29Si NMR and infrared spectroscopies, and vapor phase osmometry, J. Phys. Chem. B 101 (1997) 10638–10644.
[51] D. Dimas, I. Giannopoulou, D. Panias, Polymerization in sodium silicate solutions: a fundamental process in geopolymerization technology, J. Mater. Sci. 44 (2009) 3719–3730.
[52] O. Regev, Nucleation events during the synthesis of mesoporous materials using liquid crystalline templating, Langmuir 12 (1996) 4940–4944.
[53] C.J. Glinka, et al., Small angle neutron scattering study of the structure and formation of MCM-41 mesoporous molecular sieves, J. Porous Mater. 3 (1996) 93–98.
[54] C. Vautier-Giongo, B.L. Bales, Estimate of the ionization degree of ionic micelles based on Krafft temperature measurements, J. Phys. Chem. B 107 (2003) 5398–5403.
[55] C. La Mesa, G.A. Ranieri, M. Terenzi, Studies on Krafft point solubility in surfactant solutions, Thermochim. Acta 137 (1988) 143–150.
[56] J. Esquena, C. Rodriguez, C. Solans, H. Kunieda, Formation of mesostructured silica in nonionic fluorinated surfactant systems, Microporous Mesoporous Mater. 92 (2006) 212–219.
[57] F. Michaux, et al., In situ time-resolved SAXS study of the formation of mesostructured organically modified silica through modeling of micelles evolution during surfactant-templated self-assembly, Langmuir 28 (2012) 17477–17493.
[58] H.W. Hillhouse, J.W. Van Egmond, M. Tsapatsis, J.C. Hanson, J.Z. Larese, The interpretation of X-ray diffraction data for the determination of channel orientation in mesoporous films, Microporous Mesoporous Mater. 44 (2001) 639–643.
[59] S.A. Holt, G.J. Foran, J.W. White, Observation of hexagonal crystalline diffraction from growing silicate films, Langmuir 15 (1999) 2540–2542.
[60] T. Brennan, S.J. Roser, S. Mann, K.J. Edler, Characterization of the structure of mesoporous thin films grown at the air/water interface using X-ray surface techniques, Langmuir 19 (2003) 2639–2642.
[61] E.K. Richman, T. Brezesinski, S.H. Tolbert, Vertically oriented hexagonal mesoporous films formed through nanometre-scale epitaxy, Nat. Mater. 7 (2008) 712.
[62] K.J. Edler, J. W. Further White, Improvements in the long-range order of MCM-41 materials, Chem. Mater. 9 (1997) 1226–1233.
[63] K. Kuperkar, et al., Viscoelastic micellar water/CTAB/NaNO3 solutions: rheology, SANS and cryo-TEM analysis, J. Colloid Interface Sci. 323 (2008) 403–409.
[64] M.E. Helgeson, T.K. Hodgdon, E.W. Kaler, N.J. Wagner, A systematic study of equilibrium structure, thermodynamics, and rheology of aqueous CTAB/NaNO3 wormlike micelles, J. Colloid Interface Sci. 349 (2010) 1–12.
[65] D. Bartet, C. Gamboa, L. Sepulveda, Association of anions to cationic micelles, J. Phys. Chem. 84 (1980) 272–275.
[66] J. Frasch, B. Lebeau, M. Soulard, J. Patarin, R. Zana, In situ investigations on cetyltrimethylammonium surfactant/silicate systems, precursors of organized mesoporous MCM-41-type siliceous materials, Langmuir 16 (2000) 9049–9057.

[67] E.A. Lissi, E.B. Abuin, L. Sepulveda, F.H. Quina, Ion exchange between monovalent and divalent counterions in cationic micellar solution, J. Phys. Chem. 88 (1984) 81–85.
[68] E. Leontidis, Hofmeister anion effects on surfactant self-assembly and the formation of mesoporous solids, Curr. Opin. Colloid Interface Sci. 7 (2002) 81–91.
[69] C. Gamboa, L. Sepúlveda, High viscosities of cationic and anionic micellar solutions in the presence of added salts, J. Colloid Interface Sci. 113 (1986) 566–576.
[70] E. Cappelaere, R. Cressely, Shear banding structure in viscoelastic micellar solutions, Colloid Polym. Sci. 275 (1997) 407–418.
[71] J. Israelachvili, Intermolecular and Surface Forces, Academic Press, San Diego, CA, 1991.
[72] T. Mokhtari, et al., Controlling interfacial film formation in mixed polymer-surfactant systems by changing the vapor phase, Langmuir 30 (2014) 9991–10001.
[73] M. Thommes, Physical adsorption characterization of nanoporous materials, Chem. Ing. Tech. 82 (2010) 1059–1073.
[74] K.S.W. Sing, R.T. Williams, Physisorption hysteresis loops and the characterization of nanoporous materials, Adsorpt. Sci. Technol. 22 (2004) 773–782.
[75] E.P. Barrett, L.G. Joyner, P.P. Halenda, The determination of pore volume and area distributions in porous substances. I. Computations from nitrogen isotherms, J. Am. Chem. Soc. 73 (1951) 373–380.